The Astrophysical Journal Letters, 900:L20 (7pp), 2020 September 10 https://doi.org/10.3847/2041-8213/abafbd
© 2020. The American Astronomical Society. All rights reserved.

Optical Spectrum of the Adamantane Radical Cation

Parker Brian Crandall, David Müller, Juliette Leroux, Marko Förstel, and Otto Dopfer
Institut für Optik und Atomare Physik, Technische Universität Berlin, D-10623 Berlin, Germany; markof@physik.tu-berlin.de, dopfer@physik.tu-berlin.de
Received 2020 July 14; revised 2020 August 10; accepted 2020 August 14; published 2020 September 3

Abstract

Known for their stable structural and thermal properties, diamondoids and particularly their radical cations are viable candidates as carriers for diffuse interstellar bands. While previous research has mainly focused on neutral diamondoids and their derivatives, little is known about their radical cations, which may form in interstellar environments by ionizing radiation. We report the first experimental optical spectrum of the simplest diamondoid cation, the adamantane radical cation ($C_{10}H_{16}^+$), obtained via electronic photodissociation spectroscopy of cryogenic ions in the 310–1000 nm range. The main fragmentation channels are H loss at low energies and C_3H_7 loss at higher energies. The optical spectrum reveals a broad band spanning the range of 420–850 nm, assigned to the $D_2(^2E) \leftarrow D_0(^2A_1)$ transition using time-dependent density functional theory calculations. Despite a vibrational temperature below 20 K, we observe no vibrational structure because of lifetime broadening and/or Franck–Condon congestion. A second band system originating at 345 nm that shows vibrational progressions is attributed to the overlapping $D_5(^2A_1)/D_6(^2E) \leftarrow D_0(^2A_1)$ transitions split by the Jahn–Teller effect. The lifetime deduced from the widths of these vibronic bands is ∼30 fs. Comparison of the spectrum with known diffuse interstellar bands suggests that $C_{10}H_{16}^+$ is not likely to be a carrier. However, the strong absorption features in the UV to near-IR show promise in the investigation of higher-order diamondoids as potential candidates.

Unified Astronomy Thesaurus concepts: Astrochemistry (75); Laboratory astrophysics (2004); Interstellar medium (847); Molecular spectroscopy (2095); Diffuse interstellar bands (379); Electron impact ionization (2059); Interstellar molecules (849)

1. Introduction

Diamondoids are a class of rigid cycloalkanes that are garnering special interest in the fields of astronomy and astrochemistry. These aliphatic molecules are arranged into cage-like structures by sp^3 hybridization of the carbon atoms and are terminally saturated at the surfaces by hydrogen atoms (Dahl et al. 2003; Schwertfeger et al. 2008; Schreiner et al. 2011). With the recent discovery of fullerenes in the interstellar medium (ISM), there is an ongoing effort to interpret the spectroscopic signatures of other large, complex carbon-bearing molecules such as diamondoids and polycyclic aromatic hydrocarbons (PAHs) to compare with astronomical observations (Henning & Salama 1998; Snow et al. 1998; Tielens 2008; Knorke et al. 2009; Alata et al. 2010; Cami et al. 2010; Patzer et al. 2012; Campbell et al. 2015; George et al. 2020). The first evidence of nanodiamonds of extrasolar origin came from electron diffraction analyses of meteorites, wherein diamond material was found in concentrations of 100–400 ppm (Lewis et al. 1987). Diamondoids have not yet been confirmed to exist in the ISM. However, their structural and thermal stability suggests that they can withstand the harsh conditions of such environments and thus their detection is expected. A ubiquitous presence of diamondoids has been hypothesized and could account for more than 5% of cosmic and 40% of tertiary carbon in interstellar environments (Henning & Salama 1998). Additionally, similarities have been demonstrated between laboratory IR spectra of diamondoids and the unidentified infrared emission (UIR) bands seen in the spectra of young stars with circumstellar disks (Guillois et al. 1999; Pirali et al. 2007). Due to their low ionization energy (IE), it has also been suggested that the radical cations of these molecules, which are predicted to absorb in the IR–UV range, are present in high abundances and might be responsible for features in the well-known diffuse interstellar band (DIB) spectra (Bauschlicher et al. 2007; Steglich et al. 2011; Banerjee et al. 2015; Candian et al. 2018). The presence of DIBs in the spectra of stars has been known for just over 100 years; however, attempts to assign these bands to neutral or charged molecules over decades of laboratory spectroscopy experiments have proven to be difficult (Leach 1995; Fulara & Krelowski 2000; Jochnowitz & Maier 2008; Salama & Ehrenfreund 2014). To date, the only positively identified DIB carrier is C_{60}^+, a large caged fullerene that has been linked to 5 of the nearly 500 known bands (Campbell et al. 2015; Walker et al. 2015). Assignment of the bands at 9632 and 9577 Å was accomplished by laboratory spectra of He-tagged C_{60}^+ ions cooled in a cryogenic ion trap to temperatures relevant to the interstellar medium. Similar advanced spectroscopic methods with other fullerenes, PAHs, or large aliphatic molecules are anticipated to reveal additional assignments of DIBs (Linnartz et al. 2020).

Determining whether diamondoids and their ions have any connection to DIBs begins first with an understanding of their structural and spectroscopic properties. The simplest diamondoid, adamantane (tricyclo[3.3.1.$1^{3,7}$]decane, $C_{10}H_{16}$, Ada), has been studied thoroughly by IR (Bailey 1971; Srivastava & Singh 1979; Howard & Henry 1998; Pirali et al. 2007) and Raman spectroscopy (Bailey 1971; Jenkins & Lewis 1980; May et al. 1998; Rao et al. 2000). Additionally, ab initio calculations have explored molecular orbitals, optical absorption, and vibrational modes of neutral Ada (Jensen 2004; Bauschlicher et al. 2007; Vörös & Gali 2009). More recent emission and optical spectra from synchrotron studies report that Ada exhibits intrinsic photoluminescence in the UV and that the optical gaps and excited state decay rates of diamondoids depend on particle size (Landt et al. 2009a, 2009b; Richter et al. 2014). Much less is known about the adamantane radical cation (Ada^+), which is the focus of this work. If Ada exists in the ISM, Ada^+ is also expected because it would readily form from the neutral via ionizing radiation. A high-resolution IR photodissociation study by Patzer et al. (2012) combined with density functional theory

(DFT) calculations was the first experimental demonstration that the degenerate $^2T_2$ ground state of Ada^+ is subject to the Jahn–Teller effect and undergoes symmetry reduction from T_d to C_{3v} by elongating the C–C and C–H bonds parallel to the C_3 rotational axis. Photoelectron (PES) and total-ion-yield spectroscopy have produced low-resolution electronic spectra of Ada^+ originating from the neutral ground state of Ada and reveal experimental IEs in close agreement with the accepted value of 9.25 ± 0.04 eV (Schmidt 1973; Worley et al. 1973; Kovač & Klasinc 1978; Lenzke et al. 2007; Linstrom & Mallard 2018). Two-dimensional Penning ionization electron spectra by Tian et al. (2002) aided these early PES studies in determining the assignments of the first six bands of the PES spectrum (Table 1). While the authors of the PES studies mention the susceptibility of Ada^+ to Jahn–Teller distortion, assignments of excited states were given assuming T_d symmetry. Tian et al. (2002) were able to demonstrate the splitting of the T_1 and T_2 excited states into $E + A_2$ and $E + A_1$ states, respectively, by comparing the PES spectrum of Ada (T_d) with that of 1–chloroadamantane (C_{3v}), as well as clarify the order of closely lying states. Additionally, IR multiple-photon dissociation and threshold PES spectroscopy have explored the structures of electron ionization and photodissociation products of Ada^+ (Bouwman et al. 2018; Candian et al. 2018). Furthermore, time-dependent DFT (TD-DFT) calculations by Steglich et al. (2011) and Xiong & Saalfrank (2019) both predicted the vertical absorption spectrum of Ada^+.

Herein we report the first experimental optical spectrum of Ada^+ from the UV to near-IR range obtained by electronic photodissociation (EPD) spectroscopy. The experiments were carried out in the gas phase at cryogenic temperatures below 20 K where the ions are expected to be in their electronic and vibrational ground states. The fragmentation patterns of the parent ion were investigated by reflectron time-of-flight (ReTOF) mass spectrometry and analyzed as a function of photon frequency. The EPD spectrum is assigned by comparison to TD-DFT calculations, and the astrophysical implications, particularly those with respect to DIBs, are discussed.

2. Experimental and Computational Techniques

EPD spectra of Ada^+ were recorded in a tandem mass spectrometer equipped with a cryogenic ion trap (BerlinTrap), which has been described previously (Günther et al. 2017). For the current study, the instrument was modified with an electron ionization (EI) source to generate radical ions. The setup comprises five main chambers housing (i) the EI source to produce the ions, (ii) a hexapole ion trap for accumulation and thermalization, (iii) a quadrupole mass filter (QMS) for ion selection, (iv) a 22-pole cryogenic ion trap for storing and cooling the ions via He buffer gas, and (v) a ReTOF mass spectrometer to monitor both parent and fragment ions. The resulting EPD spectrum represents a lower limit for the optical absorption cross section, which may additionally include other deexcitation processes besides fragmentation (e.g., fluorescence). Ada crystals (99%, Sigma Aldrich) were placed in a stainless-steel tube and the ensuing Ada vapor was introduced at room temperature into the ion source, where it was bombarded by electrons emitted from a tungsten filament with a kinetic energy of 50 eV. The resulting ions were accelerated into the hexapole trap, where they were trapped and thermalized by collisions with N_2 buffer gas for 90 ms. This procedure completely removed the substantial fragmentation arising from metastable decay of hot Ada^+ ions (*m/z* 136) into adamantyl ions (*m/z* 135) by loss of H, which interfered with the desired EPD signal. After filtering through the QMS, Ada^+ ions were guided into the 22-pole cryogenic trap held at 6 K and cooled to effective vibrational ion temperatures below 20 K by He buffer gas for 90 ms (Günther et al. 2017; Müller et al. 2019). To confirm that the ions were indeed cold, the setup was tested by He tagging of CH_3^+ produced from EI of methanol, which can occur in the 22-pole trap only for ions with $T < 20$ K (Asvany et al. 2018). Cold Ada^+ ions were extracted from the 22-pole trap and guided into the extraction region of an orthogonal ReTOF mass spectrometer equipped with a microchannel plate detector. Approximately 40 μs before being deflected into the ReTOF, they were irradiated by photons with $\lambda = 310$–1000 nm emitted from a pulsed optical parametric oscillator (OPO) laser (GWU, VersaScan). The OPO laser was pumped by a nanosecond Q-switched Nd:YAG laser (Innolas, Spitlight 1000, 150 mJ/pulse at 355 nm) and delivered pulses with a beam diameter of 5 mm, a bandwidth of around 4–8 cm^{-1}, and an energy of 1–3 mJ, which was monitored online by a pyroelectric power meter. In the narrow spectral range 700–720 nm, the OPO laser power was too low for measurement. The laser system and all pulsed components of the BerlinTrap operated with a duty cycle of 10 Hz. The relative intensities of electronic transitions were determined by monitoring both parent and photofragment ions with the ReTOF mass spectrometer. At each wavelength, 100 mass spectra were averaged and linearly normalized for photon flux and parent intensity. These normalized signals were then summed and analyzed as a function of photon energy.

The experimental EPD spectra were assigned by TD-DFT calculations at the B3LYP/aug-cc-pVTZ level. To this end, the structure of the D_0 ground electronic state of Ada^+ was optimized, and vertical excitations into higher electronic doublet states (D_n with $n = 1$–6) were computed for this global minimum geometry to estimate the optical absorption spectrum of Ada^+. Unfortunately, similar to previous efforts (Xiong & Saalfrank 2019), optimization of excited states required to perform Franck–Condon simulations of vibronic transitions failed because of the multi-reference character and strong vibronic couplings arising from Jahn–Teller interactions in this highly symmetric ion. Nonetheless, the vertical excitation energies provide useful guidance for assigning the electronic states.

3. Results and Discussion

Typical mass spectra taken under various experimental settings are compared in Figure 1. Figure 1(a) represents a mass spectrum of the EI ion source taken with the laser off and the QMS set to ion guiding mode. The observed fragments match those reported for Ada in the NIST database taken at 70 eV (Linstrom & Mallard 2018) and a recent mass spectrum reported by Bouwman et al. (2018). Minor differences in relative intensities are due to a lower electron energy used herein (50 eV) and the slightly mass-dependent ion transmission of the ReTOF (which varies somewhat with the timing of the HV extraction pulses of the ReTOF). Figure 1(b) was recorded with the QMS set to transmit only Ada^+ ions (*m/z* 136), demonstrating unit mass resolution of the QMS and negligible metastable decay. The two EPD mass spectra obtained at $\lambda = 675$ and 345 nm in Figures 1(c) and (d), respectively, illustrate the energy-dependent fragmentation branching ratios. The fractional abundance of the most intense fragments was typically

Table 1
Vertical Excitation Energies (E_{vert}) for Ada^+ Computed at the TD-DFT Level (B3LYP/aug-cc-pVTZ) Compared with Previous PES Studies of Ada Highlighting the Origin of States Arising from the Jahn–Teller Splitting of Triply Degenerate T States

Worley et al. (1973)		Schmidt (1973)		Kovač & Klasinc (1978)		Tian et al. (2002)		Present Work[a]			
Position (eV)[b]	Sym	Position (eV)	Sym	Position (eV)	Sym	Position (eV)[b]	Sym	State (Sym)	E_{vert} (eV)	E_{vert} (cm^{-1})	Oscillator Strength f
9.23 (a), 9.44	T_2	9.75	T_2	9.61	T_2	9.40 (a), 9.67	T_2	D_0 ($^2A_1$)	0.0	0.0	
9.85 (a), 10.00	T_1							D_1 (^2E)	1.112	8970	0.0018
10.65 (a), 10.97	E	11.25	T_1, E	10.93	E	10.86 (a)	E	D_2 (^2E)	1.853	14946	0.0602
11.16 (a), 11.36	T_2			11.38	T_1	11.45	T_1	D_3 ($^2A_2$)	2.354	18986	0.0000
								D_4 (^2E)	2.362	19053	0.0018
12.72 (a), 12.97	T_1	13.40	T_1, T_2	12.96	T_2	13.05 (a)	T_2	D_5 ($^2A_1$)	3.847	31025	0.0623
13.15 (a), 13.54	T_2							D_6 (^2E)	3.850	31050	0.0256

Notes.
[a] The vertical excitation energies of Ada^+ differ from the PES energies of Ada by the adiabatic ionization energy of the ground state of Ada^+.
[b] Values labeled by (a) are adiabatic ionization energies and those without are vertical.

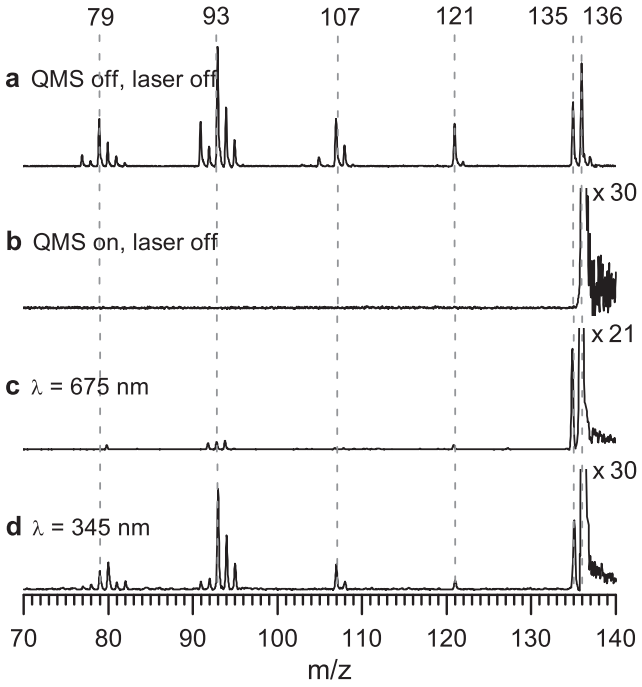

Figure 1. Reflectron time-of-flight mass spectra of Ada^+ formed by EI at 50 eV. (a) Mass spectrum of the ion source. (b) Mass spectrum of the ion source with mass selection of Ada^+ using the QMS. (c), (d) EPD mass spectra of Ada^+ obtained at 675 and 345 nm. The mass spectra in (b)–(d) are multiplied by 21 and 30 to show the weak peaks.

less than 2% of the parent ion signal. Over the spectral range of 310–1000 nm, 15 significant fragments were found at *m/z* 77–82, 91–95, 107–108, 121, and 135. The first six peaks correspond to C_4H_y losses ($y = 6$–11), with the major peak at *m/z* 79 (C_4H_9 loss). The next set of five peaks results from C_3H_x losses ($x = 4$–8), the largest peak being *m/z* 93 (C_3H_7 loss). The remaining peaks stem from C_2H_5, C_2H_4, CH_3, and H losses, respectively. A similar fragmentation pattern was observed in previous imaging photoelectron photoion coincidence (iPEPICO) mass spectra of Ada^+ (Candian et al. 2018) measured at 10.9–12.1 eV, i.e., at ionization excess energies of $E_{exc} =$ 1.7–2.81 eV above IE = 9.29 ± 0.02 eV, although individual mass peaks could not be fully resolved due to insufficient mass resolution. The mass-resolved EPD spectra are plotted in Figure 2 for several main dissociation channels, which are grouped in a similar way as in Candian et al. (2018). As expected, H loss is the dissociation channel with the lowest appearance energy (AE) of 11,100 ± 400 cm^{-1} (1.38 ± 0.05 eV), C_3H_x loss begins at 12,200 ± 400 cm^{-1} (1.51 ± 0.05 eV), while CH_3, $C_2H_{4(5)}$, and C_4H_y loss raises at 13,200 ± 500 cm^{-1} (1.64 ± 0.06 eV). These thresholds are in qualitative agreement with those reported by the iPEPICO study (1.21, 1.40, 1.54 eV), although the photoabsorption processes are different in the two experiments (resonant EPD of Ada^+ versus dissociative photoionization of Ada). Moreover, the previous results do not reflect the strong dominance of the H-loss channel at lower energies, possibly due to insufficient mass resolution. The leading dissociation channel at lower energies is H loss, peaking at 14,700 cm^{-1}, while C_3H_x loss becomes the dominant dissociation channel at energies above 16,730 cm^{-1}.

The total EPD spectrum in Figure 3 is produced by integrating the peak area for all fragments over the nearly 3500 mass spectra ($\lambda =$ 310–1000 nm at 0.2 nm resolution) and compared to the vertical absorption stick spectrum computed at the TD-DFT level (Table 1). Significantly, the EPD spectrum represents the first optical spectrum of Ada^+ and of any diamondoid cation. Compared to the optical spectrum of neutral closed-shell Ada (Landt et al. 2009b), the electronic transitions of Ada^+ are greatly redshifted by approximately 5 eV due to the radical cation character of Ada^+. An intense broad peak appears at 11,100 cm^{-1}, reaches a maximum around 14,600 cm^{-1}, and gradually decreases to a minimum near 27,200 cm^{-1}. No vibronic fine structure is observed. The band system is assigned to the second electronically excited, twofold degenerate doublet state D_2 with ^2E symmetry, predicted by TD-DFT calculations to lie at 14,946 cm^{-1} with an oscillator strength of $f = 0.0602$. This $D_2(^2E) \leftarrow D_0(^2A_1)$ transition is spin and orbitally allowed for the C_{3v} point group. Xiong & Saalfrank (2019) also employed TD-DFT calculations at the B3LYP/TZVP level for vertical excitations (because optimization of the D_2 state failed) but included vibrational Franck–Condon simulations using a restricted time-dependent wave packet approach. This approach uses the same frequencies and normal modes in the D_0 and D_2 states, neglects any Duschinsky rotation and vibronic couplings, and employs damping factors of $\Gamma = 1$, 50, 100, and 200 cm^{-1} as effective decay rates. These simulations predict for the $D_2 \leftarrow D_0$ transition a vertical energy of 1.849 eV (14,913 cm^{-1}, $f = 0.0616$) with a large width of around 0.6 eV resulting from substantial Franck–Condon activity due to the large geometry changes upon D_2 excitation. The vibronic structure is essentially unresolved for $\Gamma = 50$ cm^{-1} due to lifetime broadening (damping) and Franck–Condon congestion, with the exception of a small peak corresponding to the band origin near 1.4 eV. Our EPD spectrum closely resembles their vibronic spectra at $\Gamma = 100$ or 200 cm^{-1} except the subpeak they attribute to the adiabatic transition near 1.4 eV is not observed. Toward higher frequencies, some signal of the first band system may come from the $D_4(^2E)$ state computed with very low oscillator strength ($E_{vert} =$ 19,053 cm^{-1}, $f = 0.0018$), while the $D_3(^2A_2)$ state predicted vertically at 18,986 cm^{-1} is forbidden in C_{3v}.

A second broad and intense band system is apparent in the total EPD spectrum of Ada^+ above 28,000 cm^{-1}. TD-DFT calculations predict two optically allowed and nearly degenerate transitions in this range, namely, $D_5(^2A_1) \leftarrow D_0(^2A_1)$ at 31,025 cm^{-1} ($f =$ 0.0623) and $D_6(^2E) \leftarrow D_0(^2A_1)$ at 31,050 cm^{-1} ($f = 0.0256$), which arise from a small vertical Jahn–Teller splitting (25 cm^{-1}) of the $^2T_2$ state upon symmetry reduction from T_d to C_{3v}. Interestingly, unlike in the first band system, we observe several vibrationally resolved peaks on top of the broad feature, which are shown in more detail in Figure 4. The peaks A–E are fitted to Lorentzian line shapes with equal width yielding as best fit an FWHM = 165 ± 49 cm^{-1}, which corresponds to a lifetime of 32 ± 11 fs for the excited state. The peak maxima occur at A = 29,000 ± 15, B = 29,650 ± 16, C = 30,280 ± 15, D = 31,010 ± 18, and E = 31,560 ± 18 cm^{-1}. The relative intensities of the peaks suggest an assignment of the intense peak A to the 0–0 band origin (3.595 ± 0.002 eV, 344.9 ± 0.2 nm), which is accompanied by a short progression in a mode ν_1 with 1290 ± 21 cm^{-1} (C and E), a second fundamental mode $\nu_2 =$ 670 ± 22 cm^{-1} (B), and a combination band $\nu_1+\nu_2$ (D). Reliable supporting calculations for interpreting these vibronic features are needed but, owing to the Jahn–Teller distortion and resulting vibronic couplings of Ada^+, computational methods to converge the geometries of the excited electronic states are challenging and beyond the scope of this work.

The large width of presumably single vibronic transitions of ~160 cm^{-1} in the second band system ($D_{5/6}$) exceeds by far

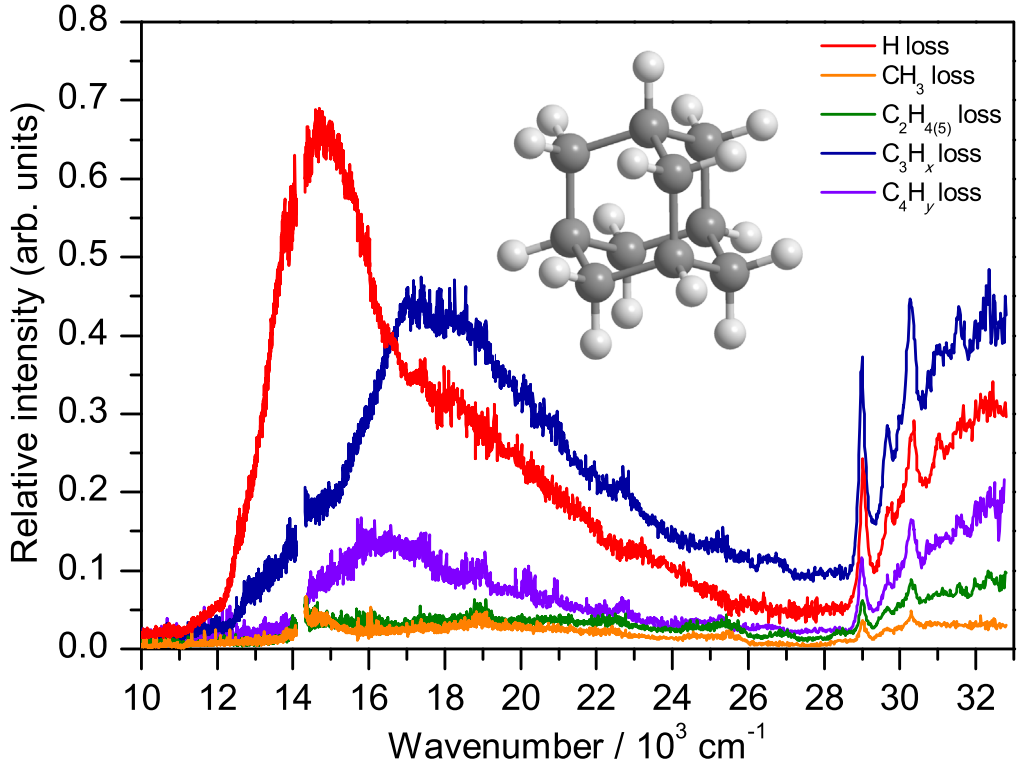

Figure 2. Mass-resolved EPD spectra of Ada^+ ($C_{10}H_{16}^+$) recorded in various fragment channels. The sum of all channels yields the total EPD spectrum shown in Figure 3. The intensities are displayed relative to the maximum value of the total EPD spectrum.

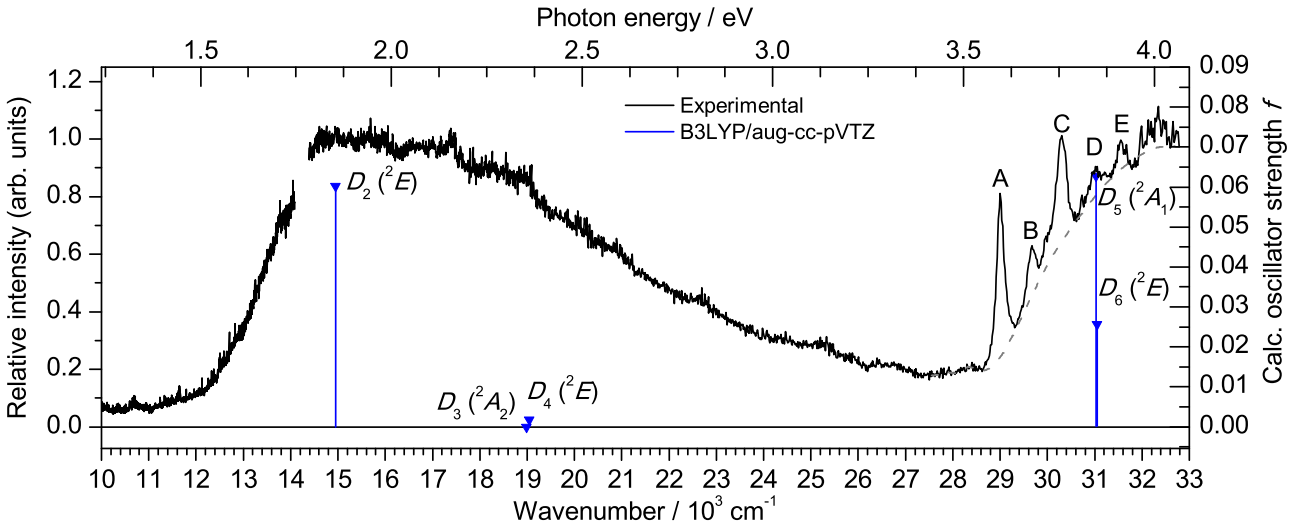

Figure 3. Total EPD spectrum of Ada^+ in the spectral range 10,000–33,000 cm^{-1} compared to stick spectra of vertical transitions of Ada^+ originating from its $^2A_1$ ground electronic state obtained by TD-DFT calculations (B3LYP/aug-cc-pVTZ; Table 1). The gray dotted line, generated using a spline from the part of the curve between the peaks, is subtracted from the spectrum to analyze the vibronic peaks (labeled A–E) in Figure 4.

both the bandwidth of the OPO laser, the rotational contour (both $<10\,cm^{-1}$), and the Jahn–Teller splitting ($25\,cm^{-1}$), and is thus predominantly attributed to lifetime broadening resulting in $\tau \sim 32 \pm 11$ fs and a decay rate of $k = (2.9 \pm 0.9) \times 10^{13}\ s^{-1}$. The $D_2 \leftarrow D_0$ spectrum is likely to be further broadened by Franck–Condon congestion of vibrational modes caused by large changes in geometry between the two states, as indicated by the simulations of this transition by Xiong & Saalfrank (2019) using various damping factors. We exclude lifetime reduction from both fluorescence (should typically be >100 ps for optically allowed transitions) and collisions with background gas (because of sufficiently low pressure). Thus, the remaining nonradiative processes are internal conversion to lower electronic states (possibly via conical intersections) and/or fast predissociation of the excited states (possibly via crossing with dissociative low-lying $\sigma\sigma^*$ states) (Sobolewski et al. 2002; Ashfold et al. 2019). In any case, the excitation energies of the whole EPD spectrum in Figure 3 lie above the dissociation threshold for H loss (1.21 eV, $9760\,cm^{-1}$; Candian et al. 2018), suggesting that single-photon absorption is energetically sufficient to drive dissociation. Because the cross section for fluorescence is

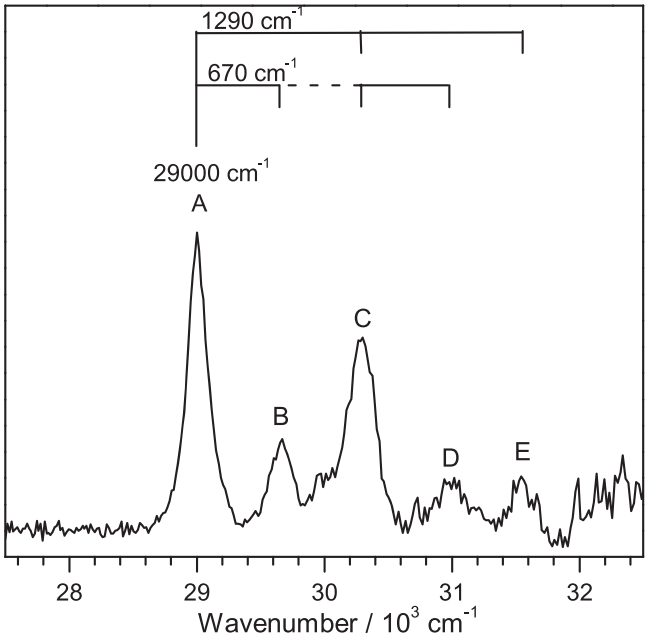

Figure 4. Expanded view of the total EPD spectrum of Ada^+ in the high frequency range (after background subtraction, Figure 3) to illustrate the vibronic progressions.

negligible, the total EPD cross section closely approximates the absorption cross section of Ada^+.

4. Conclusion and Astrophysical Implications

EPD spectroscopy reveals that the spectral features of Ada^+ representing transitions into excited electronic states are surprisingly broad even at cryogenic temperature. Previous PES studies of Ada also show broad bands in the energy range 9–15 eV, the first of which has a band origin at 9.25 eV indicating the IE of the neutral. The next two bands result from energy differences of excited states and correlate well with our EPD spectrum after accounting for the IE of Ada. In the case of these early PES spectra, however, the lower electron energy resolution, which ranges between 12–80 meV (96–640 cm^{-1}), and the elevated temperature could contribute to the broadening of spectral features. Table 1 summarizes the results of these studies and compares them to the calculated vertical transitions presented in this work at the TD-DFT (B3LYP/aug-cc-pVTZ) level of theory. The state symmetry assignments by Tian et al. (2002) are in agreement with our assignments and together demonstrate the Jahn–Teller splitting of the T_1 and T_2 states upon symmetry reduction from T_d to C_{3v}. The broadening of spectral features in the EPD spectrum is mainly attributed to the excited states exhibiting very short lifetimes. Considering the average peak width of the vibronic progression for the $D_{5/6}$ excited state(s), the decay rate is $k = (2.9 \pm 0.9) \times 10^{13}\ s^{-1}$ and implies rapid relaxation either by internal conversion to a highly excited vibrational state of the electronic ground state or via predissociation.

The primary motivation for investigating the optical properties of Ada^+ is to determine its candidacy as a DIB carrier. We show that Ada^+ decays after absorbing a photon above 850 nm and thus does not fulfill the stability requirement of a potential DIB carrier. However, it may be formed in the ISM after ionization of its very stable and optically transparent parent molecule Ada. The most current catalogs of DIBs show that the vast majority of some 500 known bands appear in the 400–800 nm range (Jenniskens & Desert 1994; Galazutdinov et al. 2000; Hobbs et al. 2008, 2009; Fan et al. 2019). Due to the immensely broad nature of the band system representing the $D_2(^2E) \leftarrow D_0(^2A_1)$ transition, we find no coincidences within this range between the Ada^+ EPD spectrum and the DIBs. Vibrationally resolved peaks are observed in the Ada^+ spectrum below 350 nm. However astronomical observations in the near-UV remain largely unexplored due to the challenges of ground-based observational methods in this range, mainly the substantial telluric ozone absorption. To the best of our knowledge, no available data in the literature reveal DIBs in close proximity and with similar widths to the vibronic peaks of the $D_5/D_6 \leftarrow D_0$ band system (Tuairisg et al. 2000; Gredel et al. 2011; Bhatt & Cami 2015; Cox et al. 2017). More astronomical observations in the near-UV are needed, particularly with low resolution as broad features could be indistinguishable in high-resolution surveys (Bhatt & Cami 2015). Additionally, while TD-DFT calculations coupled to Franck–Condon simulations are an effective computational method in simulating the optical spectra of molecules, the challenge of minimizing the geometries of excited electronic states of Ada^+ makes the assignment of vibronic features for the $D_5/D_6 \leftarrow D_0$ band system virtually impossible by this technique. More robust computational methods are required to fully interpret these bands. Although the optical spectrum of Ada^+ does not reveal any obvious resemblance to the known DIBs, the strong absorbance in the UV/Vis spectral range shows promise for higher-order diamondoid radical cations, which are to be investigated spectroscopically in the near future using the same experimental approach.

This work was supported by Deutsche Forschungsgemeinschaft (DFG, DO 729/8). The authors thank Th. Möller and A. Merli (TU Berlin) for valuable discussions and P. Saalfranck (Potsdam) for sharing his computational data.

ORCID iDs

Parker Brian Crandall https://orcid.org/0000-0002-4585-5868
Marko Förstel https://orcid.org/0000-0002-3630-9494
Otto Dopfer https://orcid.org/0000-0002-9834-4404

References

Alata, I., Omidyan, R., Broquier, M., et al. 2010, PCCP, 12, 14456
Ashfold, M. N. R., Ingle, R. A., Karsili, T. N. V., & Zhang, J. 2019, PCCP, 21, 13880
Asvany, O., Thorwirth, S., Redlich, B., & Schlemmer, S. 2018, JMoSp, 347, 1
Bailey, R. T. 1971, AcSpA, 27, 1447
Banerjee, S., Stüker, T., & Saalfrank, P. 2015, PCCP, 17, 19656
Bauschlicher, C. W., Jr., Liu, Y., Ricca, A., Mattioda, A. L., & Allamandola, L. J. 2007, ApJ, 671, 458
Bhatt, N. H., & Cami, J. 2015, ApJS, 216, 22
Bouwman, J., Horst, S., & Oomens, J. 2018, ChemPhysChem, 19, 3211
Cami, J., Bernard-Salas, J., Peeters, E., & Malek, S. E. 2010, Sci, 329, 1180
Campbell, E. K., Holz, M., Gerlich, D., & Maier, J. P. 2015, Natur, 523, 322
Candian, A., Bouwman, J., Hemberger, P., Bodi, A., & Tielens, A. G. G. M. 2018, PCCP, 20, 5399
Cox, N. L. J., Cami, J., Farhang, A., et al. 2017, A&A, 606, A76
Dahl, J. E., Liu, S. G., & Carlson, R. M. K. 2003, Sci, 299, 96
Fan, H., Hobbs, L. M., Dahlstrom, J. A., et al. 2019, ApJ, 878, 151
Fulara, J., & Krelowski, J. 2000, NewAR, 44, 581
Galazutdinov, G. A., Musaev, F. A., Krełowski, J., & Walker, G. A. H. 2000, PASP, 112, 648
George, M. A. R., Förstel, M., & Dopfer, O. 2020, Angew. Chem., 59, 12098
Gredel, R., Carpentier, Y., Rouillé, G., et al. 2011, A&A, 530, A26
Guillois, O., Ledoux, G., & Reynaud, C. 1999, ApJL, 521, L133

Günther, A., Nieto, P., Müller, D., et al. 2017, JMoSp, 332, 8
Henning, T., & Salama, F. 1998, Sci, 282, 2204
Hobbs, L. M., York, D. G., Snow, T. P., et al. 2008, ApJ, 680, 1256
Hobbs, L. M., York, D. G., Thorburn, J. A., et al. 2009, ApJ, 705, 32
Howard, D. L., & Henry, B. R. 1998, JPCA, 102, 561
Jenkins, T. E., & Lewis, J. 1980, AcSpA, 36, 259
Jenniskens, P., & Desert, F. 1994, A&AS, 106, 39
Jensen, J. O. 2004, AcSpA, 60, 1895
Jochnowitz, E. B., & Maier, J. P. 2008, MolPh, 106, 2093
Knorke, H., Langer, J., Oomens, J., & Dopfer, O. 2009, ApJ, 706, 66
Kovač, B., & Klasinc, L. 1978, Croat. Chem. Acta, 51, 55, https://hrcak.srce.hr/195979
Landt, L., Kielich, W., Wolter, D., et al. 2009a, PhRvB, 80, 205323
Landt, L., Klünder, K., Dahl, J. E., et al. 2009b, PhRvL, 103, 047402
Leach, S. 1995, P&SS, 43, 1153
Lenzke, K., Landt, L., Hoener, M., et al. 2007, JChPh, 127, 084320
Lewis, R. S., Ming, T., Wacker, J. F., Anders, E., & Steel, E. 1987, Natur, 326, 160
Linnartz, H., Cami, J., Cordiner, M., et al. 2020, JMoSp, 367, 111243
Linstrom, P. J., & Mallard, W. J. 2018, NIST Chemistry WebBook (Gaithersburg, MD: NIST), https://webbook.nist.gov/chemistry/
May, P. W., Ashworth, S. H., Pickard, C. D. O., et al. 1998, PhysChemComm, 1, 35
Müller, D., Nieto, P., Miyazaki, M., & Dopfer, O. 2019, FaDi, 217, 256
Patzer, A., Schütz, M., Möller, T., & Dopfer, O. 2012, Angew. Chem., 51, 4925
Pirali, O., Vervloet, M., Dahl, J. E., et al. 2007, ApJ, 661, 919
Rao, R., Sakuntala, T., Deb, S. K., et al. 2000, JChPh, 112, 6739
Richter, R., Wolter, D., Zimmermann, T., et al. 2014, PCCP, 16, 3070
Salama, F., & Ehrenfreund, P. 2014, in IAU Symp. 297, The Diffuse Interstellar Bands, ed. J. Cami & N. L. J. Cox (Cambridge: Cambridge Univ. Press), 364
Schmidt, W. 1973, Tetrahedron, 29, 2129
Schreiner, P. R., Chernish, L. V., Gunchenko, P. A., et al. 2011, Natur, 477, 308
Schwertfeger, H., Fokin, A. A., & Schreiner, P. R. 2008, Angew. Chem., 47, 1022
Snow, T. P., le Page, V., Keheyan, Y., & Bierbaum, V. M. 1998, Natur, 391, 259
Sobolewski, A. L., Domcke, W., Dedonder-Lardeux, C., & Jouvet, C. 2002, PCCP, 4, 1093
Srivastava, S. P., & Singh, I. D. 1979, Acta Phys. Acad. Sci. Hung., 47, 275
Steglich, M., Huisken, F., Dahl, J. E., Carlson, R. M. K., & Henning, T. 2011, ApJ, 729, 91
Tian, S. X., Kishimoto, N., & Ohno, K. 2002, JPCA, 106, 6541
Tielens, A. G. G. M. 2008, ARA&A, 46, 289
Tuairisg, S. Ó, Cami, J., Foing, B. H., Sonnentrucker, P., & Ehrenfreund, P. 2000, A&AS, 142, 225
Vörös, M., & Gali, A. 2009, PhRvB, 80, 161411
Walker, G. A. H., Bohlender, D. A., Maier, J. P., & Campbell, E. K. 2015, ApJL, 812, L8
Worley, S. D., Mateescu, G. D., McFarland, C. W., Fort, R. C., & Sheleyld, C. F. 1973, J. Am. Chem. Soc., 95, 7580
Xiong, T., & Saalfrank, P. 2019, JPCA, 123, 8871